Influence of snow properties, air flow and design on structure-borne snowdrifts at Neumayer Station III

Océane Hames[1,2], Mahdi Jafari[2], Peter Köhler[3], Christian Haas[3,4] and Michael Lehning[1,2]

[1]School of Architecture, Civil and Environmental Engineering, Ecole Polytechnique Fédérale de Lausanne (EPFL), Lausanne, Switzerland
[2]WSL Institute for Snow and Avalanche Research SLF, Davos, Switzerland
[3]Alfred-Wegener-Institut (AWI), Helmholtz-Zentrum für Polar- und Meeresforschung, Bremerhaven, Germany
[4]Institute for Environmental Physics (IUP), University of Bremen, Bremen, Germany

Key Points:

- Our numerical model is able to reproduce the main snowdrift components measured around the German Antarctic research station Neumayer III
- Wind force, bed intercohesion, snowfall and fine changes in the structure shape have a strong impact on snowdrift locations and quantities
- Those parameters should be incorporated in snow transport models for an accurate evaluation of drifting snow around complex structures

Corresponding author: Océane Hames, hames.oceane@gmail.com

Abstract

The genesis of snowdrifts and its governing processes are not fully understood. Yet, the assessment of snow redistribution by the wind is essential in snow-affected regions for risk management, water resources and mitigation tactics. Factors such as flow turbulence and snow properties showed to be crucial for the snow-wind interaction on flat terrain. In this work, we add a third component and investigate the drifting mechanisms of snow around complex building structures using numerical Euler-Lagrange simulations. The German Antarctic research station Neumayer III is investigated in particular. Results show that structure-borne snowdrifts are strongly influenced by the wind forcing, precipitation, snow cohesion and fine changes in the obstacle shape. Thus, these factors should be cautiously included in numerical models simulating snow transport at small scales.

Plain Language Summary

In cold regions, snow is present for a (more or less) large fraction of the year and accumulates around various structures that deviate the wind from its trajectory. The snow piling up under the form of snowdrifts can engender large costs and logistic difficulties, especially in urbanized areas. However, the environmental and architectural factors that influence snowdrifts are not fully understood. The present work aims to identify the parameters that affect snow accumulation around structures using a numerical snow transport model. Due to its location in the Antarctic, the German research station Neumayer III was chosen as an example site and simulations were run for this building in particular. Results show that the wind speed, snow particle characteristics and subtle features of the obstacle shape could largely influence snowdrifts. Thus, those parameters should be included in small-scale snow transport models as well as in the development of snow mitigation strategies.

1 Introduction

Snow-covered surfaces are often eroded by the wind in alpine and polar regions. The areas where snow gets eroded or deposited strongly depend on the terrain topography and its interaction with the wind. Aeolian snow transport is a process of major importance in snow-affected regions as it strongly influences the height distribution, micro-structure and mass balance of the snow (Mott et al., 2018). In Antarctica, substantial snow transport is observed from the inner plateau to the coast due to large-scale katabatic winds, creating clouds of blowing snow with a height of hundreds of meters (Palm et al., 2017). Thus, the snow relocates over an extremely large terrain (Lenaerts & van den Broeke, 2012) and typically forms sastrugis or wind sculptured snow dunes of various shapes and extents (Amory et al., 2017; Sommer et al., 2018).

The aeolian transport of particles is classified into three processes, each governed by distinct physical phenomena: creep, saltation and suspension (Bagnold, 1941). Creep is the rolling or sliding of particles along the surface at a height below ∼0.01 m. Saltation describes the motion of particles close to the surface (0.01-0.1 m), following short ballistic trajectories. Saltating grains may eject other particles when colliding with the bed. Suspension is the transport of particles that are sufficiently small to be lifted to greater heights by turbulent eddies. Grains in suspension travel large distances without contact with the ground and usually reach heights of 0.1-100 m (Lehning et al., 2008). The terms drifting and blowing snow are often used to indicate, respectively, the movement of snow particles close to the surface (up to 2 m height) and the movement of smaller snow particles transported at high elevations (Melo et al., 2022).

Saltation is an important snow drifting mechanism and is considered to accomplish the bulk of snow mass transport. It is estimated to account for about 50–75% of all snow particle movement by the wind (Gromke et al., 2014; Dai & Huang, 2014). Saltation is

initiated by three distinct modes: aerodynamic entrainment, rebound and ejection. Aerodynamic entrainment occurs when particles initially at the surface are picked up by aerodynamic forces only. The particle mass flux and concentration are expected to increase with surface shear stress, as previously observed in simulations and field measurements (Nishimura et al., 2014; Melo et al., 2022). Rebound happens when particles hit the ground and bounce to a new ballistic trajectory. Ejection (or splash) occurs when particles laying in the ground are launched into saltation due to the impact of saltating particles (Doorschot & Lehning, 2002). Different authors contributed to the physical understanding of these saltation modes and developed parametrizations for the wind-particle-bed interaction on flat terrain. We particularly refer to Comola and Lehning (2017), who proposed splash laws based on conservation principles to describe saltation as well as Melo et al. (2024), who recently investigated the physical validity of diverse saltation models.

Complexity is added to snow drifting processes in the presence of aerodynamic obstacles, due to the separation of airflow at their sharp edges and corners. Extensive snowdrifts with scouring and deposition are typically observed around built structures in urbanized snowy regions (Tominaga et al., 2011). In Antarctica, the windswept conditions cause the snow to accumulate around research stations and other man-made structures. The generated snowdrifts remain permanent fixtures due to the extreme cold climate and can only be removed by human intervention or additional snow scouring. This continuous snow accumulation enhanced by limited snow melt can reduce the useful life of structures that may become completely buried, inaccessible or unsafe (Beyers, 2004). For such cases, studies on snow drifting around obstacles are of great significance. Obstacle shapes, snow particle properties, meteorological conditions and surroundings are all expected to have a significant impact on the wind field and snowdrifts around structures (Zhou & Zhang, 2023). However, the exact contribution of each of these processes has not been rigorously investigated. In this context, Zhou and Zhang (2023) have encouraged researchers to conduct systematic studies on snow drifting around obstacles. Numerical tools to quantitatively predict snow accumulation around obstacles have been presented in the past (Uematsu et al., 1991; Beyers, 2004) but are not generally accepted or sufficiently validated.

In this work, we investigate snow transport and accumulation around obstacles using computational fluid dynamics (CFD) simulations. Two main CFD methods have been used to simulate snowdrift around obstacles in the literature, namely the Eulerian-Eulerian (E-E) and the Eulerian-Lagrangian (E-L) methods. Both solve the continuous air phase using the flow governing equations, but they handle the snow phase differently. In the E-E method, snow is regarded as a continuous phase and its motion is resolved using convective-diffusive transport equations (Schneiderbauer & Prokop, 2011). Alternatively, the E-L approach considers snow as a discrete phase and tracks the trajectories of each particle (or group of particles) separately (Tominaga et al., 2011; Zhou & Zhang, 2023). Until now, the E-L approach has been widely used to study snow transport on flat terrain (Groot Zwaaftink et al., 2013; Melo et al., 2022), but was rarely applied to research on snow drifting around obstacles due to its high computing costs (Zhou & Zhang, 2023; Chen & Yu, 2023). Our snow transport model is based on the Eulerian-Lagrangian method and entails a detailed representation of snow grain dynamics at the surface by including the three saltation initiation modes (Hames et al., 2022). It is well suitable for the exploration of snow drifting mechanisms as it is able to simulate particle behavior from a microscopic perspective.

This manuscript explores the intrinsic mechanisms of snow drifting around complex structures with the detailed snow transport model snowBedFoam (Hames et al., 2021). The German Antarctic research station Neumayer III (Wesche et al., 2016) is used as an exemplary site due to the substantial snow accumulation it experiences. To our knowledge, past literature has not used a fully detailed Eulerian-Lagrangian model to study snow drifting mechanisms around such complex structures. Parameters connected to flow tur-

bulence, snow properties and structure design are varied in our numerical simulations to emphasize their effect on snow redistribution. The final goal is to identify the governing processes of snowdrift and understand which parameters are crucial to include in modeling frameworks.

First, the Neumayer III research station and its associated snow accumulation are described in Section 2. Then, a description of the snow transport model (Section 3.1), numerics (Section 3.2), and simulation sets (Section 3.3) follows. Finally, the results are presented (Section 4) and discussed in the last section (Section 5).

2 Data

2.1 Neumayer Station III

The present work investigates the snow accumulation around the German research station Neumayer III in Dronning Maud Land, Antarctica (70°40'S and 08°16'W). It was inaugurated on February 20, 2009 as the new German Antarctic research base. It is operated by the Alfred Wegener Institute (AWI), Helmholtz Centre for Polar and Marine Research and follows the Georg-von-Neumayer Station (1981-1992) and Neumayer II Station (1992-2009) as the German overwintering station on the Ekström Ice Shelf (Wesche et al., 2016). Neumayer Station III (hereafter referred to as Neumayer station) integrates research, operational and accommodation facilities in one building. It is situated on a wooden platform above the snow surface and stands on 16 hydraulic pillars (6 meters) that are regularly adjusted to the changes in snow cover. A garage below the station offers shelter for polar vehicles (Wesche et al., 2016). Figure 1.A shows the location of Neumayer station on the Antarctic continent. The two pictures on the right hand side present a scheme of the internal station layout (B) and a recent photograph of the building (C).

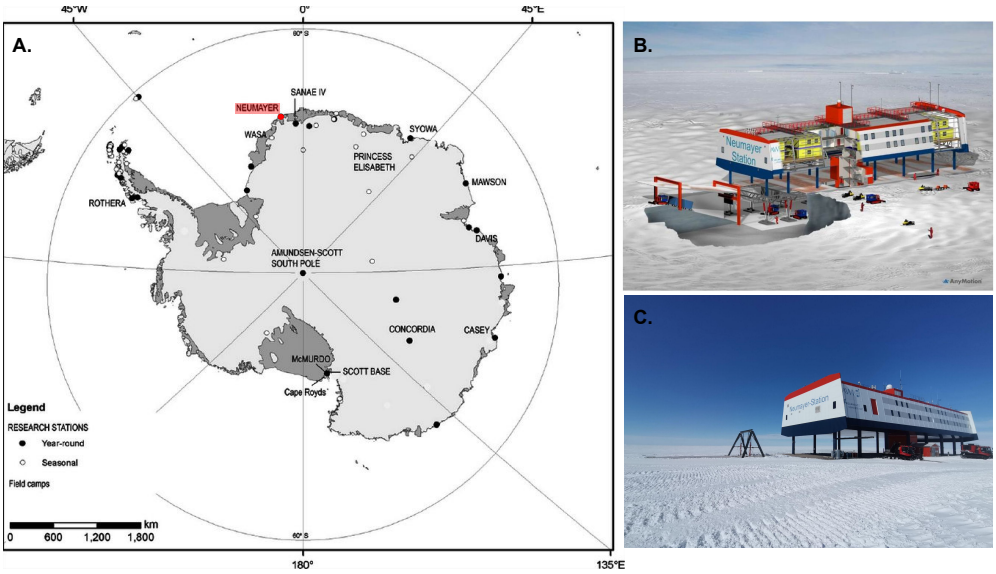

Figure 1. **A.** Map of the Antarctic continent and location of the German research station Neumayer III (in red). **B.** Scheme of the internal layout of Neumayer station III. **C.** Recent photograph of Neumayer Station III (November 2022).

Due to its location close to the coast (ca. 20 km from the ice shelf edge on the Ekström Ice Shelf), weather and climate at Neumayer station are characterized by relatively high wind speeds, with an annual mean value of 8.7 $m.s^{-1}$ (Bagheri Dastgerdi et al., 2021).

Complex dynamical processes caused by travelling cyclones and katabatic winds give rise to large variations in wind speed and wind direction (Kottmeier & Fay, 1998). Two main wind directions are observed at Neumayer station. The prevailing one is from the east, caused by the passage of cyclones north of the Antarctic coast. Easterly storms with wind speeds of up to approx. 40 $m.s^{-1}$ are frequently observed and bring most of the snowfall. The second, less common typical wind direction is south to south-west, caused by a mixture of weak katabatic and synoptic influence, with typical wind speeds below 10 $m.s^{-1}$ (König-Langlo et al., 1998). The proximity of open waters leads to more important precipitation compared to locations inside the continent. Similarly to other coastal stations, blowing and drifting snow is often observed and reported in 40% of all visual observations (König-Langlo & Loose, 2007).

For the design plan of Neumayer Station III, an extensive study on the aerodynamic behavior of the building was carried out by Leitl et al. (2006). Snowdrift and wind pressure distributions were studied for various configurations using scaled wind tunnel models. It was found that a trapezoidal shape for the station contour provides technological and aerodynamic advantages over the other tested designs. However, despite the efforts to minimize its capture, snow started to accumulate in the direct vicinity of the building, forming two typical snowdrifts on each side of the station along the predominant wind direction (Figure 4.I). Every snowstorm has brought the special challenge of excess snow accumulation, needing to be continuously removed to prevent the burial of the station (S. Franke et al., 2022). It is estimated that about 10,000 m^3 of snow are displaced annually by the snow groomers. These specific conditions make Neumayer station an ideal site to investigate the genesis of snowdrifts. The recurrent snow blizzards occurring in the region generate numerous events that can help understand the environmental conditions leading to the formation of snowdrifts, as well as their quantitative effects.

2.2 Snowdrift measurements

The station construction in 2009 was rapidly followed by the development of an important adjoining snowdrift. The latter shows a characteristic structure with a single, restrained hill on the East side (windward) and two elongated hills on the West side (leeward). The drifts look similar at present, although reaching a greater height. The snow topography formed by 3 months of accumulation after the station opening was surveyed with barometric measurements taken on a regularly spaced grid (Figure 4.I). The overwintering staff who first observed the snow accumulation at the station developed a method to derive snow height based on fine pressure measurements. Two precision barometers were used to record the pressure and the longitude/latitude coordinates were determined with a GPS receiver (average of 4 measurements with a 1 s resolution). The final grid has a horizontal resolution of 5 m in the North-South axis and 10 m in the East-West axis. The accuracy of the height measurements is expected to be around 30 cm.

This barometrically-derived snow map is used as a verification dataset for the numerical simulations performed in this work. It shows the snow accumulation stemming from storms of various intensities and directions. From February to June 2009, measurements at the station showed a mean wind direction of 103° relative to North and an average wind speed of 9.2 $m.s^{-1}$ (at 10 m) (Schmithüsen, 2020). The highest recorded wind speeds (above 10 $m.s^{-1}$) had an average direction of 93°. Although storms at Neumayer mostly come from the East, there were still high wind speed events (Schmithüsen, 2020) likely to have redistributed the deposited snow around the station in other directions. Note that a part of the snow accumulation in the direct vicinity of the station was removed by the overwintering staff for safety and logistical purposes. Moreover, quantitative estimates of snowfall are non existent for the measurement period. Although not suitable for a fully quantitative validation, these measurements are useful to understand the typical snowdrift structure that formed over time around Neumayer station.

3 Methods

3.1 Snow transport model

To simulate snow distribution around Neumayer station, we make use of a multi-phase CFD solver implemented in the open-source software OpenFOAM (Christopher J. Greenshields, CFD Direct Ltd., 2023) called snowBedFoam (Hames et al., 2021). Based on the finite volume method (FVM) (Moukalled et al., 2015), it handles coupled Eulerian and Lagrangian phases, which involves a finite number of particles spread in a continuous phase. The solver tracks the motions of all (agglomerates of) particles at the micro-mechanical level, based on the so-called Lagrangian particle tracking (LPT) method. In snowBedFoam, the Eulerian continuum equations including particle volume fraction are solved for the fluid phase, whereas Newton's equations for motion are solved to determine the particles trajectories. The generic Eulerian and Lagrangian equations implemented in the DPMFoam solver can be found in various publications, as well as in the source code (OpenFOAM Foundation Ltd., 2018; Fernandes et al., 2018).

For the sake of conciseness, we only provide an overview of the snow transport model employed in the simulations. The equations governing the snow and fluid systems are thoroughly described in previous publications (Sharma et al., 2018; Melo et al., 2022; Hames et al., 2022) and we refer to those for additional details. In snowBedFoam, the implemented equations parametrize the three main modes of saltation initiation (i.e. aerodynamic entrainment, rebound and splash). Aerodynamic entrainment occurs when the wind flow has sufficient momentum to lift up particles from the surface. The amount of eroded particles is determined using Bagnold's shear stress threshold (Bagnold, 1941) and a parametrization developed by Anderson and Haff (1991). Once a snow particle is present in the fluid, it might hit the surface upon which it can not only rebound, but also eject other particles from the bed to the overlying fluid. In snowBedFoam, rebound entrainment is modelled using a rebound probability developed by Anderson and Haff (1991) and adapted to snow based on the work of various authors (Doorschot & Lehning, 2002; Groot Zwaaftink et al., 2013). The equations for splash entrainment were developed by Comola and Lehning (2017); they depend on bed cohesion, particle diameter and velocity, particle ejection angles and impact energy (momentum) fractions. All combined, these parametrizations determine the amount of snow particles being displaced from the snowbed to the overlying air (and inversely). They represent in details the complex wind-particle, but also particle-particle interactions found in nature.

3.2 Numerics

3.2.1 Numerical domain

Figure 2 shows the numerical domain employed for our simulations. The Neumayer station building was simulated with its real dimensions, namely 68 (L) x 24 (W) x 20 (H) m. Its 16 hydraulic pillars reach a height of 6 m, and their hexagonal shape was approximated with a 1 m squared base. The building staircase was also included in the model, with a size of 14 (L) x 5 (W) x 6 (H) m and a triangular end at one side (Figure 3.A). The staircase is elongated perpendicularly to the longest axis of the station. The building is oriented in the domain such that our simulations represent the direction of the most significant storms observed at Neumayer station (East). The numerical domain extent was determined based on the building height. The longitudinal extension of the domain in front (approach flow) reaches 200 m (10 H), which is slightly bigger than the 8 H recommended by Bartzis et al. (2004) for known approach flow profiles. The extension of the region behind the station (wake) reaches 300 m (15 H) to allow for flow re-development behind the wake region, in accordance with J. Franke and Baklanov (2007). Some building details were overlooked to simplify the geometry and the subsequent meshing process. We made sure to use enough elements to capture the finest building structures (pillars). The cells around the building reach a final size of about 10 cm, while the ones in

the far-away field reach a maximum size of 2 m. The first grid point in the near-wall boundary layer is located at about 0.75 cm in the wall-normal direction. To reduce the number of grid points, we applied a wall function computing the shear stress between the wall and the first computational node. The latter was placed at a non-dimensional wall distance between 30 and 500 for a valid use of the wall function (J. Franke & Baklanov, 2007). The number of elements in the final meshes varies between 8 and 9 million cells.

3.2.2 Turbulence and discretization

In our snow simulations, we use a statistically steady description of a neutrally-stratified turbulent flow by solving the Reynolds Averaged Navier-Stokes (RANS) equations (Pope, 2000). The Reynolds stress tensor is computed using the standard two-equation closure model k-ϵ, which solves two additional transport equations for turbulent kinetic energy (k) and turbulent dissipation rate (ϵ). More information about the k-ϵ model can be found in the introductory paper by Launder and Spalding (1974). The turbulence model in RANS must represent a very wide range of scales and is expected to perform poorly when used to calculate separating or free shear flows. However, it is computationally less expensive than other turbulence models such as Large-Eddy Simulation (LES) (de Villiers, 2006). For the modeling of snowdrift around structures, most fluid dynamics studies have employed the RANS equations approach assuming that averaged flows are sufficient to predict the main erosion and deposition zones (Tominaga et al., 2011; Tominaga, 2018; Zhou et al., 2020). However, as pointed out by Tominaga (2018), it is important to take into account the instantaneous turbulent flow structures that generate particle sweep and ejection events in snowdrift modeling. This may mean that RANS approaches are not suitable and LES is required to extract non-isotropic three-dimensional velocity fluctuations. However, the effects of turbulent motions in snowdrift simulations are not clear and further investigation is needed, which is out of the scope of the present work.

Looking at numerical schemes, the gradient and divergence terms in the conservation equations were discretized using the Gauss linear and bounded Gauss linear upwind schemes, respectively. The Euler method was employed for the discretization of the transient terms (Moukalled et al., 2015). For the flow time step, we make use of an automatic control called "*adjustableRunTime*" available in OpenFOAM, which adapts the time step based on a maximum Courant number value defined by the user. The Courant number as the stability criterion is defined as the product of fluid velocity and time step divided by the numerical cell length scale. More information regarding the adjustable time step method for the flow is available in Jafari et al. (2022).

3.2.3 Boundary conditions and initialization

The boundary conditions (BCs) set in the simulations are shown in Figure 2.A for the fluid and particle phases. The flow conditions are shown for each patch in the white upper boxes. A fully developed atmospheric boundary layer profile was applied at the inlet (red), with the wind speed specified at 10 m height. A pressure outlet condition was applied at the outlet patch (green), while the lateral patches (purple) were assigned symmetry. Symmetry conditions enforce a parallel flow by requiring a vanishing normal velocity component at the boundary; the latter was positioned far enough from the bluff body to avoid any artificial flow acceleration. No-slip BC was used for the velocities at the snowbed (blue) and station (pink) walls, while zero-gradient was used at the top boundary. The chosen boundary conditions are in line with the best practice guidelines for the CFD simulation of flows in the urban environment developed by J. Franke and Baklanov (2007).

The boundary conditions for particles are shown for each patch in the light green lower boxes. The aerodynamic entrainment and rebound-splash modules are activated for the snowbed (ground) patch only. Around the station, the initial particle concentration at

the surface is defined so that there is never a shortage in the supply of erodible particles (Melo et al., 2022). However, the initial particle concentration is set to zero directly under the station to mimic the wooden panel on which it stands in reality. At the station wall, particles are set to rebound while they escape the domain at the lateral and top boundaries.

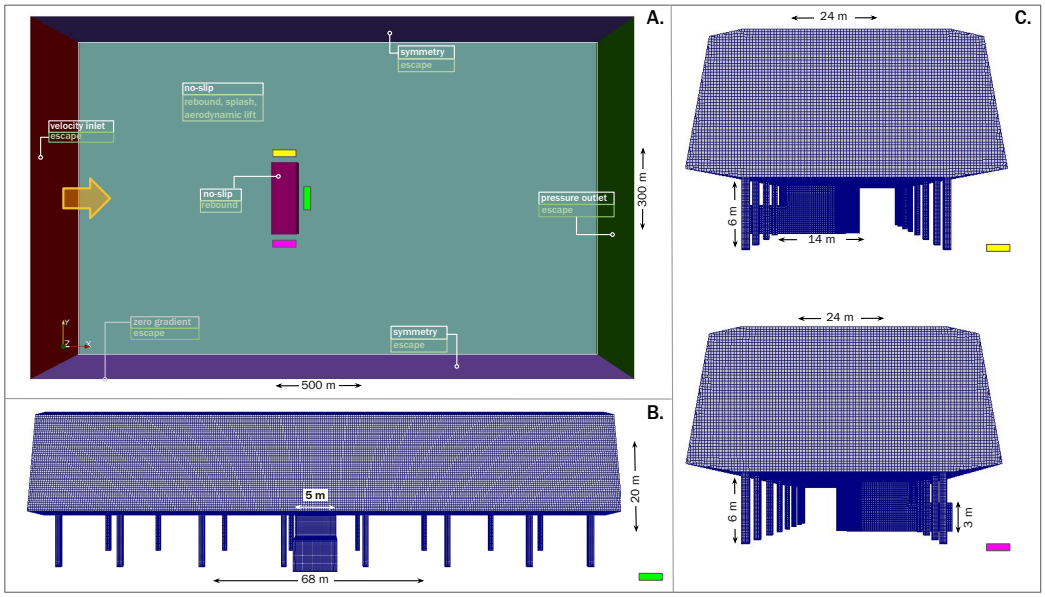

Figure 2. **A.** Numerical domain used for the snowBedFoam simulations, with the chosen boundary conditions per patch. The station building is represented in pink. Words in light green relate to particles boundary conditions, while other colours (white, light grey) are connected to the fluid. The flow direction is indicated by the orange arrow. **B.** Front view (from green rectangle in sub-panel A) and dimensions of the Neumayer station numerical model used in the simulations. **C.** Side views (from yellow and pink rectangles in sub-panel A) and dimensions of the Neumayer station numerical model used in the simulations.

To ensure stability, all our simulations were initialized with flow-fields computed with the above-mentioned boundary conditions, but without turbulence. Then, purely Eulerian simulations were run for 100 s to obtain fully developed wind-fields. The latter ultimately served as starting points for the Eulerian-Lagrangian simulations with full snow particle surface dynamics.

3.2.4 Particle dynamics

In order to reduce the computational costs, particles were grouped in parcels made of particles with similar size and trajectory. Particles from the same parcel were aerodynamically entrained at the same surface location and time step, or were ejected from the same impact event. The number of particles per parcel can assume a value between 5,000 and 250,000 (Melo et al., 2022). We chose a value of 25,000 for our snow transport simulations because it provides results that are similar to those obtained with 5,000 particles per parcel, but at lower computational cost. For simplicity, only gravity and fluid-particle drag forces were considered to solve the grain trajectories; we neglect the other small particle–fluid interaction forces commonly found in nature as well as the inter-particle collisional forces (Tominaga et al., 2011; Zhou & Zhang, 2023).

For each parcel location, the Eulerian quantities are defined using the "*cellPointWallModified*" method that linearly interpolates the closest cell point values with inverse distance weighing; in addition, Eulerian vectors (e.g. velocity) on domain boundaries are extrapolated from the cell center values and modified in such a way that they do not point out of the domain (Leonard et al., 2021). In OpenFOAM, the parcel motion is captured using a "face-to-face tracking algorithm" that adapts the Lagrangian time step depending on the crossed cell boundaries (Macpherson et al., 2009). In a first phase, the particles enter the domain by aerodynamic entrainment. Once there are snow parcels aloft in the air, the rebound-splash module is called each time a parcel hits the snow surface, resolving the micro-scale ejection processes of snow grains at the bed.

3.2.5 Reference settings

Series of simulations were performed in this work, whose reference settings are given in Table 1. If not stipulated otherwise, one should assume that the performed simulations have the numerical characteristics shown below. To investigate the governing processes of snowdrift formation, the base parameters were successively varied and their effect on the simulation results highlighted (Section 3.3).

Table 1. Reference numerical settings for the snowBedFoam simulation series.

Variable	**Symbol**	**Name/Value**	**Unit**
Turbulence model	–	k-ϵ	–
Turbulent viscosity	ν_f	1.5 $\times 10^{-5}$	$m^2.s^{-1}$
Air density	ρ_f	1.4	$kg.m^{-3}$
Wind speed (10 m)	WS	7.8	$m.s^{-1}$
Wind direction (10 m)	WD	90	$^\circ$
Particle density	ρ_p	918.4	$kg.m^{-3}$
Particle diameter (mean)	d_m	150	μm
Particle diameter (min)	d_{min}	50	μm
Particle diameter (max)	d_{max}	500	μm
Particle diameter (deviation)	σ_d	50	μm
Bed cohesion	ϕ	10^{-10}	J
Kinetic energy fraction (rebound)	ϵ_r	0.25	–
Momentum fraction (rebound)	μ_r	$\sqrt{\epsilon_r}$	–
Kinetic energy fraction (friction)	ϵ_f	0.96 $(1-P_r\epsilon_r)$	–
Momentum fraction (friction)	μ_f	0.4	–
Station orientation	–	0	$^\circ$
Staircase shape	–	triangle	–
Pillar height	–	6	m
Flow initialization	–	100	s
Simulation time	–	500	s

The wind speed was chosen such that snow particles can be aerodynamically lifted due to a surface shear stress superior to Bagnold's shear stress threshold (Bagnold, 1941; Sharma et al., 2018). The wind direction is representative of the most significant storms at Neumayer station (East) (König-Langlo & Loose, 2007). For the snow phase, values chosen for the particle properties and rebound-splash models were based on simulations ran by Melo et al. (2022): they stem from the most established values in the literature. The simulation time was set to ensure that the Eulerian-Lagrangian simulations reached a steady-

state, i.e. with the aloft particle mass not varying more than 10% over the last 100 s of simulation. The station shape and pillar height comply with the real building characteristics.

3.3 Simulation sets

The sets of snowBedFoam simulations performed in this work are presented subsequently. After a first comparison of the numerical results with in situ snowdrift measurements (Section 3.3.1), each of the factors presumed to influence snowdrift formation is investigated in details (Section 3.3.2). Note that Table 3 gives an overview of all the simulations and eases the interpretation of the results presented in Section 4.

3.3.1 Model validation

We seek to numerically reproduce the barometric snowdrift measurements taken in June 2009 after the station opening (Figure 4.I). The snow accumulation has caused the surface topography to evolve over time, having direct feedback on the wind speed and direction. Such interactions between the wind field and snowdrift formation need to be considered to precisely simulate snowdrift formation and evolution over long time periods (Komatsu & Nishimura, 2022). Our model does not comprehend a time-evolving numerical surface. Hence, we compare the snow distribution in a qualitative manner and verify that our snow model is able to reproduce the main snowdrift components. Quantities are only compared relatively.

The forcing parameters for the validation simulations were derived from meteorological observations at Neumayer Station III (Schmithüsen, 2020). Boundary conditions at the inflow (velocity-inlet) were based on the average wind speed and direction of the most significant wind events measured from February 20 to June 11, 2009. The exact values are reported in Table 2. The term "significant wind events" means that only wind speeds above 10 $m.s^{-1}$ were selected to compute the forcing values. This threshold is based on observations at Neumayer station, which show that snow begins to drift at wind speeds of 6-12 $m.s^{-1}$ depending on the conditions (König-Langlo & Loose, 2007). Precipitation particles were injected at the inlet to mimic preferential deposition, which is known to impact small-scale snow distribution in complex terrain (Lehning et al., 2008). Snowfall estimates at Neumayer are not available for the period of interest, thus a standard value of 1 $mm.h^{-1}$ was set. The station building is oriented 356° relative to North. In our simulations, the inflow is kept parallel to the lateral boundaries to stay in accordance with the symmetry boundary conditions. Therefore, any wind direction different from 90° (Eastern wind) is taken into account by rotating the building relatively to the windfields. The building orientation combined with the measured average wind direction result in a total building rotation of 7° in the validation simulations.

Table 2. Average wind speed and direction of the most significant wind events (above 10 $m.s^{-1}$) measured at Neumayer Station III from February to June 2009. The directions are given relative to North.

Wind speed [m/s]	Wind direction [°]	Building orientation [°]
16.3	93	356

3.3.2 Sensitivity analysis

Besides the comparison to measurements, several simulation series were run to individually investigate the factors influencing snowdrift, with Neumayer III as a test site. The chosen set-ups are related to the three major processes that showed to affect structure-borne snowdrifts (Pomeroy & Gray, 1990; Doorschot & Lehning, 2002; Melo et al., 2022; Tominaga, 2018): (1) flow and turbulence, (2) snow properties and (3) obstacle design. Table 3 gives an overview of each simulations series, sorted by process and described more thoroughly hereafter.

Table 3. Simulation series investigating the effects of flow and turbulence (FLOW), snow properties (SNOW) and obstacle design (STRUCT) on structure-borne snowdrifts.

Reference	**Tested parameter**	**Value**
	Flow and turbulence	
FLOW1.1	Turbulence effect	rotation = 5°
FLOW1.2	Turbulence effect	rotation = −5°
FLOW2.1	Friction velocity	u* = 0.2 m.s^{-1}
FLOW2.2	Friction velocity	u* = 0.4 m.s^{-1}
FLOW2.3	Friction velocity	u* = 0.6 m.s^{-1}
	Snow properties	
SNOW1.1	Particle diameter	d_m = 150 μm
SNOW1.2	Particle diameter	d_m = 200 μm
SNOW1.3	Particle diameter	d_m = 250 μm
SNOW2.1	Precipitation	I = 0.5 mm.h^{-1}
SNOW2.2	Precipitation	I = 1.0 mm.h^{-1}
SNOW3.1	Bed inter-cohesion	ϕ = 0 J
SNOW3.2	Bed inter-cohesion	ϕ = 5 $\times 10^{-10}$ J
SNOW3.3	Bed inter-cohesion	ϕ = 5 $\times 10^{-9}$ J
	Structure design	
STRUCT1.1	Pillar height	H_{pillar} = 4 m
STRUCT1.2	Pillar height	H_{pillar} = 6 m
STRUCT1.3	Pillar height	H_{pillar} = 8 m
STRUCT2.1	Staircase shape	no staircase
STRUCT2.2	Staircase shape	triangular
STRUCT2.3	Staircase shape	rectangular
STRUCT2.4	Staircase shape	rounded

Flow and turbulence [FLOW]

Our snow simulations show small-scale distribution patterns with very distinct erosion features (streaks) that are unlikely to be found in nature (Section 4). The Earth's atmosphere is inherently turbulent and contains local unsteadiness (eddies) that are not explicitly predicted with ensemble-averaged equations such as in the RANS method (Pope, 2000). The intermittent dynamics observed in turbulent flows and their associated snow transport are only partially represented in our simulations. For example, the lateral motions of large eddy structures are not well resolved. The FLOW1 simulations aim to show the effect that large-scale turbulence would have on the simulated snow distribution patterns. For this purpose, two simulations are performed with the standard settings except for a slight building rotation of 5° (one in each direction). This slight change in ori-

entation should mimic the effect of intermittent variations in wind direction caused by atmospheric turbulence. They are referred to as FLOW1.1 and FLOW1.2 in Table 3.

Besides atmospheric turbulence, wind speed and the associated surface shear forces are known to strongly impact snow saltation and suspension (Nishimura et al., 2014; Sharma et al., 2018). Snow transport rates have shown to increase with the square (Pomeroy & Gray, 1990) or even the cube of the friction velocity (u*) (Bagnold, 1941). Thus, u* is expected to substantially affect snow transport. The FLOW2 simulations explore its effect on the snowdrift properties, using friction velocities of 0.2, 0.4 and 0.6 $m.s^{-1}$. The other settings stay unchanged and comply with Table 1.

Snow properties [SNOW]

The mean particle diameter is expected to affect the particle concentrations and velocities in the air. Based on wind tunnel experiments performed on uniform sand beds with various grain diameters, Bagnold (1941) found that the saltation mass flux is proportional to the square root of the grain size. The numerical model of Doorschot and Lehning (2002) also predicts an increase in the integrated mass flux with the grain diameter. On the other hand, numerical results from Melo et al. (2022) show a negligible variation of the snow mass flux with d_m. Note that these studies were performed on flat terrain. Hence, the connection between mean snow grain diameter and saltation fluxes is unclear. We test the effect of particle diameter on structure-borne snowdrifts by varying the grain size to 150 μm, 200 μm and 250 μm in our SNOW1 simulations. The standard deviation, minimum and maximum particle diameter are kept constant (Table 1). The mean grain size is presumed to have an impact on snow accumulation quantities.

In addition to grain size, turbulent wind-fields are known to influence the deposition of precipitation particles by acting on their settling velocities in a process called preferential deposition (Lehning et al., 2008). The flow deflection created by an obstacle is expected to decrease, respectively enhance, the deposition of snowfall in particular locations. The effect of preferential deposition on small-scale snowdrifts is investigated in the SNOW2 simulations by adding precipitation particles in the numerical domain at intensities of 0.5 and 1 $mm.h^{-1}$, respectively. Those values correspond to light and moderate snowfall according to the classification of Rasmussen et al. (1999). The presence of snowfall is expected to enhance snow accumulation in zones of low kinetic energy.

Within the surface, snow grains are inter-connected and create bounds with each other that strengthen over time (Sharma et al., 2019). This process called sintering is represented in our snow transport model via the bed cohesion energy parameter (ϕ) (Comola & Lehning, 2017). Its influence on snowdrifts is investigated in our simulations by setting no bed cohesion (0 J) and bed cohesion at different energy levels (5×10^{-10} J, 5×10^{-9} J). Those values are similar to the ones tested by Melo et al. (2022) when investigating snow cohesion effects on saltation fluxes. The authors found that higher bed cohesion can decrease snow saltation mass fluxes at low friction velocities, while it increases snow transport at higher friction velocities in a non-monotonous way. Compared to flat terrain, the flow-field around obstacles is largely deflected and the friction velocities vary from low (wake zone) to high (structure sides). Hence, the effect of ϕ on snowdrift quantities is ambiguous. The SNOW3 simulations aim to shed light on the link between snow accumulation and bed cohesion properties.

Structure design [STRUCT]

The STRUCT simulations differ from the previous ones in the sense that they look at the influence of the structure (obstacle) parameters on snowdrifts rather than at the effect of environmental conditions. Years of scientific research on snowdrift since the institution of Antarctic stations have set the ground for the development of general construction guidelines for polar buildings. In particular, Melbourne and Styles (1969) conducted wind-tunnel experiments to understand the link between building design and snow

drifting. Among others, they found that the height of elevated buildings was important to minimise the occurrence of snow accumulation. Hence, the height of the 16 station pillars at Neumayer could have an influence on the wind speed-up under the building and on the subsequent snow scouring and deposition. To understand the effect of pillar height on snowdrifts, simulations with height values of 4, 6 and 8 m were successively tested in the STRUCT1 series. The dimensions of the pillar base (1 x 1 m) are kept constant.

Besides ground-to-building height, observations combined with wind-tunnel experiments have highlighted the importance of the building staircase on the snow accumulation at Neumayer III. Results obtained from wind-tunnel experiments without a staircase (Leitl et al., 2006) turned out to be very different from the real snowdrift conditions at the station with stairs. Thus, the presence (or not) of a staircase structure is expected to have a strong influence on the snow distribution patterns around the station. Moreover, various authors (e.g. Tominaga et al. (2011); Leitl et al. (2006)) showed the importance of the shape of buildings on snow accumulation. In particular, rounded windward corners of obstacles have shown to mitigate snow deposition (Melbourne & Styles, 1969). Since observations suggest that the staircase has a major impact on the snowdrifts born from Neumayer, our STRUCT2 simulations investigate the influence of (i) its presence and (ii) the shape of its windward corners, when present. The geometry of the windward-facing section of the staircase was successively changed from a triangular shape to rectangular and rounded shapes. Note that only the shape of the 3 m end of the staircase was changed, while its overall dimensions (14 x 5 x 6 m) were kept constant. Figure 3 illustrates the differences in design that were tested in the simulations.

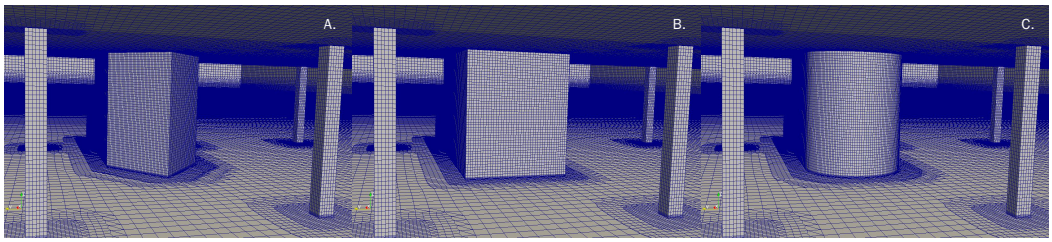

Figure 3. Overview of the staircase shapes at the windward side employed in the STRUCT2 simulation series. **A.** Triangle shape (reference), **B.** Rectangle shape and **C.** Rounded shape.

4 Results

4.1 Model validation

The simulation with measurement-based boundary conditions described in Section 3.3.1 aims to show the ability of our snowBedFoam model to reproduce snow distribution patterns born from the complex Neumayer structure. Figure 4.I shows the barometric measurements of the snowdrift, while Figure 4.II shows the snow distribution results simulated with the average wind conditions of the strongest wind events (> 10 m/s) measured from February to June 2009 (Schmithüsen, 2020). Despite the limited measurement resolution, the main components of the snowdrift around the Neumayer building are captured and we aim to verify whether our numerical model is able to reproduce them.

The snow distribution patterns in Figure 4.II display locations of snow erosion in blue and locations of deposition (snowdrift) in red. A similar color scale is used for the sensitivity results hereafter. The simulation results were oriented such that the station is facing the same direction as the measurements (building aligned with the geographic North).

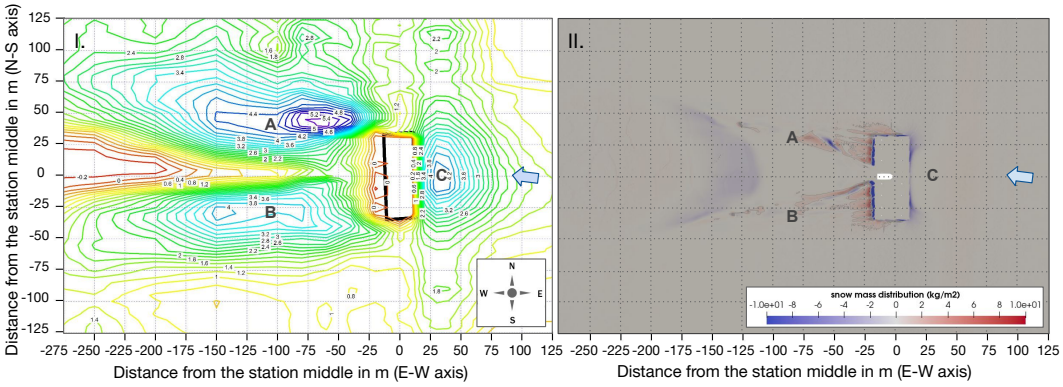

Figure 4. **I.** Characteristic snowdrift topography around Neumayer Station III, barometrically measured on June 11, 2009 over an area of 400 by 250 meters. The isolines show the topography structure in meters. **II.** Simulation results obtained with the average wind speed/direction of the most significant wind events during February to June 2009 at the inflow and considering a station orientation of 356° relative to North. The wind direction is represented by the blue arrow. The snow deposition is represented in red, while the erosion is shown in blue.

The measured snowdrift is made of two main components: (1) a small-sized hill on the East (windward) side (**C**); (2) two larger, elongated drifts on the West (lee) side (**A**, **B**). These features are visible in the simulations. Analyzing the snowdrifts along the flow stream (East to West), the first deposition area in the measurements appears at the East side of the station in the direct vicinity of the building. In the simulation, the maximum deposition location upwind appears about 50 m away from the station while it is closer in the measurements ($\sim$ 25 m). The hill is expected to shift towards the station over time as the snow accumulates and forms a new obstacle to the wind-fields. Such behaviour has been previously described with numerical simulations (Liston et al., 1993) but is not reproduced in our model with a constant numerical surface. Moreover, simulations with the same (measured) wind direction but a lower wind speed of 10 m.s^{-1} showed that the snow accumulation in **C** gets nearer to the building (Figure A1, Appendix). This suggests that the lower range of wind speeds initiating drifting snow conditions are likely to enhance the accumulation at the East (windward) side. Previous findings by Comola et al. (2019) show similar results, with different deposition patterns emerging from different combinations of reference length scale, obstacle size, friction velocity and reference velocity. Each combination is characterized by a specific interaction between particle inertia, flow advection, and gravity that affect the deposition process of snow grains. Besides, looking at the stations sides, the erosion in the simulations (near **C**) can be identified in the observations with the sharp height decrease near the building.

At the opposite side of the station, the measurements show a zero height in the direct lee (West) that smoothly increases towards the two snow hills (**A**, **B**). This feature mainly accounts for the human work (snow removal and leveling). Further downstream, the two hills in the lee side appear clearly in both the measurements and simulations (**A**, **B**). They seem to emerge from the combination of two phenomena: (1) the erosion of snow at the station sides and its subsequent deposition in adjacent wake zones, responsible for the nearest accumulation to the station; (2) the sheltering of snowfall by the station under predominant wind conditions (East). This prevents the fallen snow from being transported away by the wind and allows it to accumulate and cohere at specific locations under the form of permanent structures. The extent of the two western hills is smaller in the numerical results compared to measurements; since we only simulate one wind direction,

slight changes in this parameter would cause the snow to redistribute and the hills to expand in all directions (see simulations below, Figure 5). As the measured topography results from storms of various directions and turbulence, this leads to the more smooth snow deposition patterns observed. Moreover, the two western hills around Neumayer have most likely grown further downstream over time due to the reciprocal influence of the accumulated snow on the wind-fields. As our model only simulates the initial snow accumulation after the station inauguration (flat ground), it is expected that the snowdrifts do not elongate in the flow direction as much as in the measurements. At last, the erosion zone in the lee of the two western hills is present in both model and measurements and results from the equilibrium between the fluid and snow phases that is reached again after the Neumayer obstacle. Overall, model and measurements are qualitatively comparable and we consider the model able to reproduce the main snowdrift components around complex structures.

4.2 Sensitivity analysis

In this section, the results are rotated by ∼180 ° compared to the validation simulations. This orientation is more intuitive because it follows the direction of the airflow from left to right along the domain x-axis, such as in Figure 2.A. Thus, the plots hereafter show the patterns from the windward (left) to the leeward side (right) of the station. The name and settings of the simulations mentioned hereafter are listed in Table 3.

4.2.1 Flow and turbulence

Turbulence effect

Figure 5 shows the results for the FLOW1.1 and FLOW1.2 simulations, which demonstrate the effect of lateral turbulence on the snow distribution patterns. The two left panels show the snow distribution results obtained with a slight rotation (± 5°) replicating the effect of intermittent deviations in wind direction caused by large-scale eddies. Some erosion streaks emerging from the pillars are visible in both simulations. They were also observed in wind-tunnel experiments around Neumayer station conducted by Leitl et al. (2006). The symmetry boundary conditions in our numerical simulations enforce parallel flow (Section 3.2.3) and act similarly to wind-tunnel walls. The flow is strictly directed towards the outlet in both cases, and the obtained snow distributions stem from a constant, single wind direction. Such conditions do not exist in natural flows where the snow gets redistributed in various places due to the irregular breakdown of large vortices. Hence, overwinterers at Neumayer station have not observed any trace of the pillar influence in the snowdrift around the building. We sought to reproduce the snow accumulation that would occur under naturally turbulent flows by combining results of various flow directions together. The right panel of Figure 5 shows the snow distribution patterns obtained by combining the two ± 5° rotations together with the non-rotated reference simulations. The blue erosion streaks obtained with single wind directions are fading away in the averaged patterns, which suggests that snowdrifts get smoothed out by large-scale turbulence under natural conditions. It should be kept in mind that our results stem from idealized numerical simulations that amplify the emergence of striated patterns unlikely to be found in the real environment.

Friction velocity

Figure 6 shows the snow distribution results obtained with various friction velocities (0.2, 0.4, 0.6 $m.s^{-1}$). Note that the color scales vary for each simulation due to large differences in drifted quantities. We progressively compare the FLOW2 simulations in the flow direction, from left to right. At the windward side, the snow accumulation in **C** is nonexistent for FLOW2.1 ($u^* = 0.2$ $m.s^{-1}$), while it increases and gets closer to the station building at higher friction velocities. Greater momentum enables the wind to carry

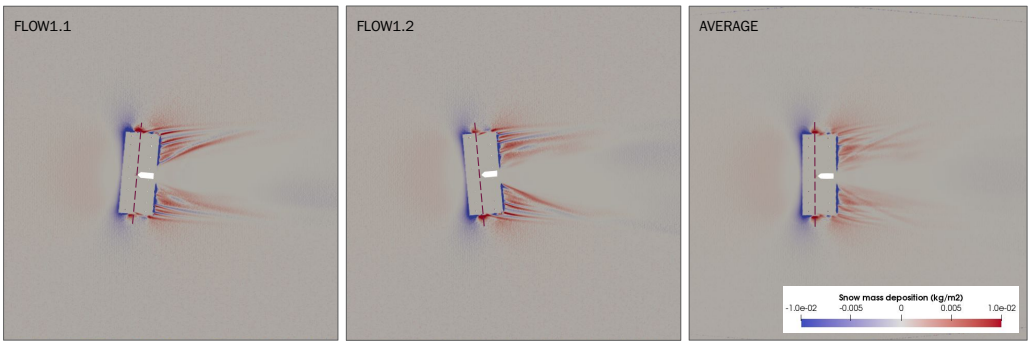

Figure 5. Snow distribution results obtained with the standard settings and a 5° rotation (FLOW1.1) as well as a −5° rotation (FLOW1.2). The right panel shows the snow distribution patterns obtained by averaging results obtained with the reference settings and the FLOW1.1/FLOW1.2 setups. The air flows from left to right.

more particles, which subsequently deposit when the flow gets blocked by the station. From the FLOW2.2 to the FLOW2.3 simulations, the extent of the snow accumulation zone in the lateral direction reduces and is replaced by erosion (**D**). Both a higher surface friction velocity and a higher number of particles aloft in the air (higher ejection) for the FLOW2.3 simulation can explain those differences. At the lee side, the surface area of the two main snowdrifts (**A**, **B**) increases with u*, while the extent of the erosion zone right behind the building in the flow direction (**E**) decreases. The flow erodes particles at the station edge in amounts that are proportional to the shear stress it exerts on the ground. The conveyed particles act as a momentum sink and reduce the snow mass that the fluid is able to carry, which creates deposition in the lee directly after the erosion occurred. In the FLOW2.1 simulations, less particles are carried and a greater distance is necessary to reach the transition point between erosion and deposition. The evolution of surface friction velocity over time after the start of particle erosion is shown in the supplementary material of Sharma et al. (2018) (Figure S2) for three different wind forcing values. The authors noticed that the rate at which the surface friction velocity decays is dependent on the forcing; larger forcing showed to decay more rapidly to the equilibrium surface velocity value. Our results are in line with those observations and suggest that the turning point at which the erosion of particles in **E** switches to deposition occurs faster (smaller distance needed to decrease flow strength) at higher u* (FLOW2.3). In addition, in the FLOW2.2/3 simulations, the erosion zone right behind the building is followed by an area with deposition hot spots. Sharma et al. (2018) showed that the mass difference between the times when the air lifts up particles and when it reaches equilibrium increases with u* (Figure S1 of their supplementary material). At the lowest u*, the authors obtain a mass difference that is almost null. Similarly, our results only show deposition hot spots after the erosion zone **E** for the simulations with a higher u*, which translates that there was some mass in excess in the air compared to the equilibrium snow mass.

In terms of snow deposition amounts, there is a factor 36 between the average deposition obtained for the FLOW2.1 and FLOW2.2 simulations, which becomes a factor 3 from the FLOW2.2 to the FLOW2.3 results. The deposited quantities vary importantly between the cases, most likely due to the fact that the friction velocity in the FLOW2.1

simulation (u* = 0.2 m.s^{-1}) is close to the surface shear stress threshold defined in the aerodynamic lift entrainment module (Sharma et al., 2018; Melo et al., 2022; Hames et al., 2022). In addition, the wind forcing influences the distribution of snow erosion and deposition quantities. At u* = 0.6 m.s^{-1}, the proportion of cells showing low erosion is greater than those showing low deposition. However, there is a larger proportion of cells showing high deposition than high erosion. In sum, our results suggest that the friction velocity impacts the snow distribution both in terms of patterns and proportions; it can be recognized as an important component of the snow drifting processes.

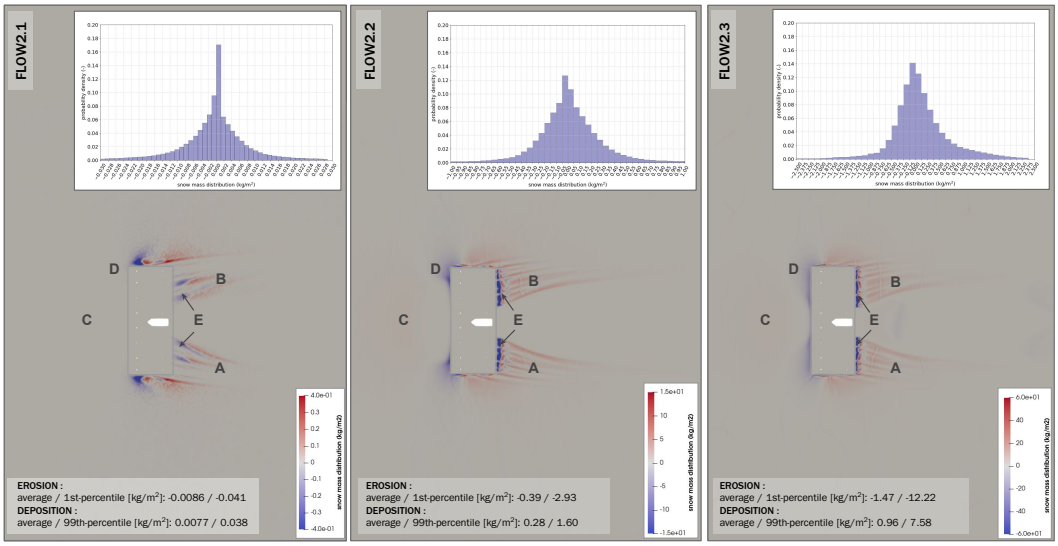

Figure 6. Snow distribution results obtained with the standard settings and a friction velocity of u* = 0.2 m.s^{-1} (FLOW2.1), u* = 0.4 m.s^{-1} (FLOW2.2) and u* = 0.6 m.s^{-1} (FLOW2.3). The air flows from left to right. The top right plots show the probability distribution of snow erosion and deposition. Statistics for deposition and erosion are shown in the bottom left corner.

4.2.2 Snow properties

Particle diameter

Figure 7 shows the snow distribution results obtained with various particle diameters (150, 200, 250 μm). The drift patterns are quite similar between the simulations: the snow deposits at the same locations (**A**, **B**). Yet, the erosion patterns at the windward side (**D**) are more distinguishable. For the highest particle diameter (d_m = 250 μm, SNOW1.3), the erosion streaks laterally spread over larger distances, which could be due to a stronger ejection process. In the lee of the station, the transition from erosion to deposition (**E**) occurs closer to the building for the larger particles, most likely due to the greater momentum they extract from the flow. Right after the erosion in the lee of the building, there are zones of stronger deposition in the SNOW1.2-1.3 simulations. The ability of the flow to accelerate saltating grains reduces with particle mass (Melo et al., 2022), thus a lower particle velocity could cause an anticipated deposition of the grains.

Quantitatively speaking, the effect of particle diameter on snowdrift size appears to be non-monotonous. The SNOW1.2 simulation (d_m = 200 μm) shows the largest mean deposition and erosion values, which are about 25% and 15% larger than the simulations with the lowest and highest particle diameter, respectively. They also show the highest

1st and 99th percentiles. The higher erosion in SNOW1.2 compared to SNOW1.1 can be explained by the splash process: the number of ejected particles is directly proportional to the cube of the particle diameter. At the highest particle diameter (SNOW1.3), there is an overall decrease of particles aloft in the air due to a lower aerodynamic entrainment (higher shear stress threshold). This difference also appears in the histograms, where more than 30% of the SNOW1.3 distribution corresponds to limited erosion. All of these observations explain why the highest erosion (and subsequent deposition) occurs for medium-sized particles.

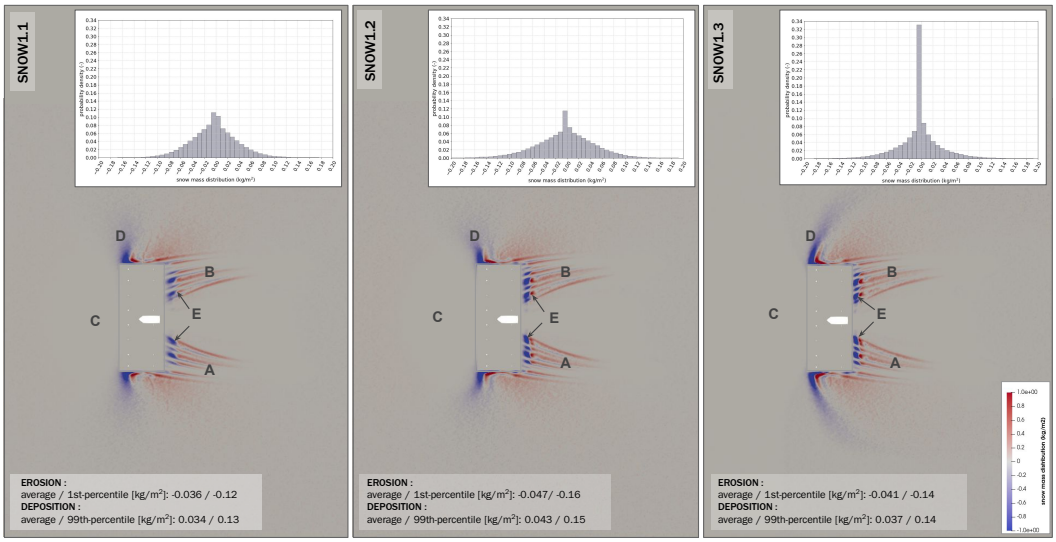

Figure 7. Snow distribution results obtained with the standard settings and particle diameter of $d_m = 150$ μm (SNOW1.1), $d_m = 200$ μm (SNOW1.2) and $d_m = 250$ μm (SNOW1.3). The air flows from left to right. The top right plots show the probability distribution of snow erosion and deposition. Statistics for deposition and erosion are shown in the bottom left corner.

Precipitation

Figure 8 shows the snow distribution patterns simulated with the standard settings and snowfall of various intensities (0, 0.5, 1 mm.h^{-1}) injected uniformly from the inlet boundary (Figure 2.A). Overall, there is more deposition on the numerical surface due to the injection of precipitation particles in the domain. At the windward side, the snow accumulation increases with snowfall intensity and becomes a predominant feature of the drift (**C**). The simulations with solely drifting snow (SNOW1.1) show the windward deposition maximum further away from the building. Once that saltating particles enter the low-speed zone induced by the station, they cannot be carried further and quickly deposit. However, precipitation particles are located higher in the air and can deposit closer to the station along their falling trajectory. This effect called preferential deposition (Lehning et al., 2008; Comola et al., 2019; Huang et al., 2024) seems to importantly impact the intensity of the snow deposition at the windward side. Beneath the station, there are more snow grains depositing windward from the staircase and from the pillars (**F**) as snowfall increases. The higher number of particles in the air increases their chance to get trapped in the low-velocity zones created by the building components. In the lee of the station, the extent of the erosion zone (**E**) decreases with an increasing snowfall intensity. The bigger amount of particles in the air extracts more momentum and decreases the shear stress of the fluid together with its ability to erode particles at the surface. Both the magnitude and surface area of the two main snowdrift structures at the

lee side (**A**, **B**) rise with snowfall intensity. Snow also accumulates in the direct lee of the staircase (between **A** and **B**) due to particles reaching this sheltered region from above.

On the quantitative side, the histograms shift to the right (deposition) and become positively skewed in the presence of snowfall. From the SNOW1.1 to the SNOW2.2 set-up, the average snow deposition increases by 55% and the 99th percentile by 40%. The erosion stays relatively stable and increases by 10% on average for SNOW2.2. This augmentation is most likely due to an enhanced ejection of snow grains by falling particles at the surface. Thus, precipitation is important both in terms of snow distribution location (windward drift) and quantities.

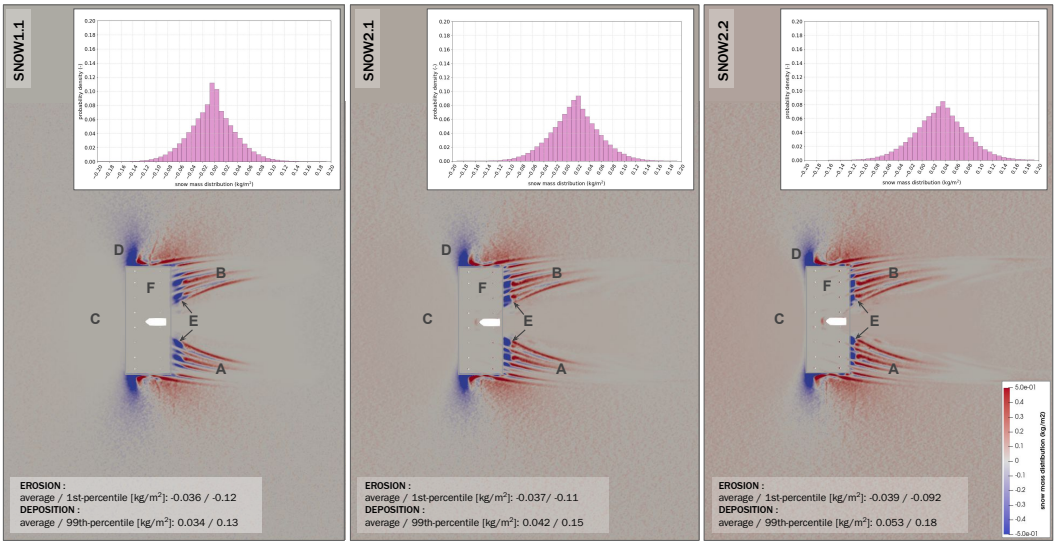

Figure 8. Snow distribution results obtained with the standard settings and precipitation values of I = 0 mm.h^{-1} (SNOW1.1), I = 0.5 mm.h^{-1} (SNOW2.1) and I = 1 mm.h^{-1} (SNOW2.2). The air flows from left to right. The top right plots show the probability distribution of snow erosion and deposition. Statistics for deposition and erosion are shown in the bottom left corner.

Bed inter-cohesion

Figure 9 shows the snow distribution results obtained with different bed inter-cohesion values (SNOW3) involved in the rebound-splash module of snowBedFoam (Comola & Lehning, 2017) and chosen based on simulations by Melo et al. (2022). The qualitative results are shown with the same range of -0.1 to 0.1 kg.m^2, while the histograms on the top right have different scales for more clarity. The snow distribution patterns show that the range of snow mass distribution values is very different from one case to the other; those discrepancies can be directly investigated in the histograms. For the simulations without bed inter-cohesion (SNOW3.1), the average erosion and deposition values are -0.076 and 0.065 kg.m^{-2}, respectively. This is about twice the values obtained with the reference settings ($\phi = 10^{-10}$ J) and 40 times the values obtained with the highest bed inter-cohesion energy (SNOW3.3, $\phi = 5 \times 10^{-9}$ J). Thus, the bed inter-cohesion parameter has a great impact in terms of drifting snow quantities.

In terms of locations of erosion and deposition, the main snowdrift components are present in all simulations (**A**, **B**, **C**). At the leeward side, the erosion zone right behind the building (**E**) is importantly reduced in the SNOW3.3 simulations, likely due to a reduced ejec-

tion process. Moreover, an asymmetry appears at the lee side (**B**) in the simulations with higher cohesion values (SNOW3.2, SNOW3.3). The station staircase is not exactly centered in between the pillars, which causes the difference in the leeward snowdrift patterns. Figure A2 (Appendix) shows the surface friction velocity patterns obtained without inter-particle cohesion, and with $\phi = 5 \times 10^{-9}$ J. As the air exits the station underside, it picks up particles that act as a momentum sink and cause a decrease in streamwise wind speed (thus surface friction velocity) directly in the lee of the station. With lower inter-particle cohesion, the wind speed decrease is more drastic because there are more particles aloft and the shear force applied to the surface accordingly decreases downstream of the station (no high velocity streaks). With higher inter-particle cohesion, the wind speed stays high enough to show the effects of the stair asymmetry in the flow and snow patterns. Those results are in line with wind-tunnel experiments conducted by Okaze et al. (2012), which showed that the near-surface wind velocities over a loose snow surface were lower than that over a hard snow surface. Thus, a lower inter-particle cohesion in the snowbed smooths out the wind speed variations caused by the station geometry and qualitatively impacts the snowdrifts.

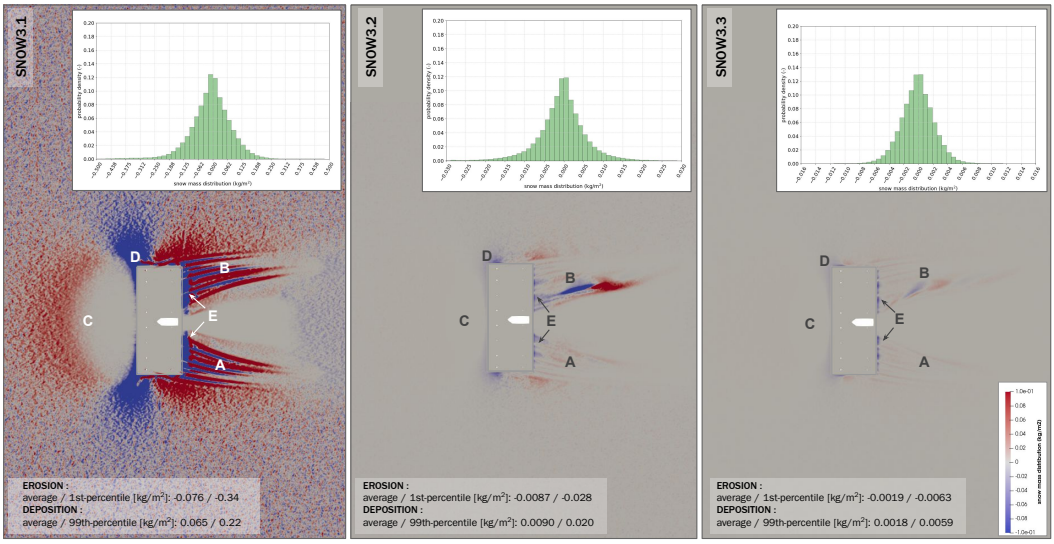

Figure 9. Snow distribution results obtained with the standard settings and bed inter-cohesion values of $\phi = 0$ J (SNOW3.1), $\phi = 5 \times 10^{-10}$ J (SNOW3.2) and $\phi = 5 \times 10^{-9}$ J (SNOW3.3). The air flows from left to right. The top right plots show the probability distribution of snow erosion and deposition. Statistics for deposition and erosion are shown in the bottom left corner.

4.2.3 Structure design

Pillar height

Figure 10 shows the snow distribution results obtained with a pillar height of 4 m (STRUCT1.1), 6 m (STRUCT1.2) and 8 m (STRUCT1.3). Qualitatively, the snow distribution patterns do not vary much. The snow deposition is slightly more important at the sides (**F**) for the smallest pillar height; those simulations also show a snow free area that is a little larger directly in the lee of the staircase (the sides of snowdrifts **A** and **B** are further away from each other). The maximum erosion (-3.7 kg.m^{-2}) and deposition values (2.7 kg.m^{-2})

are 30% higher for the lowest pillars compared to the STRUCT1.2 and STRUCT1.3 simulations. These differences can be explained by a higher flow speed-up (jet effect) under the station. On the other hand, the average deposition is the lowest for the 4 m pillars and represents about 30% of the value obtained for the standard pillar height (6 m). The latter shows the largest mean deposition value (0.034 kg.m^{-2}) of all STRUCT1 simulations, which is about 15% higher than the 8 m pillar simulations. Both stay similar in terms of percentiles.

Surface distribution plots of friction velocity (Figure A3) shed light on the non-linear relationship noticed between average deposition/erosion values and pillar height. The STRUCT1.1 simulations show a higher speed-up under the station, causing the higher maximum snow erosion (deposition) values obtained. On the other hand, its higher speed causes the flow to be more strongly deviated to the sides by the staircase (straight trajectory). This explains the smaller snow deposition surface area found in the lee of the station. For the 6 m pillar height (STRUCT1.2), the flow is less importantly accelerated and able to penetrate in between the staircase and its adjoining pillars; this increases the surface area affected by snow erosion and deposition. For the highest pillar height, the flow has an even lower acceleration and is more importantly blocked by the staircase and its 2 adjacent pillars, creating again a larger wake area in the station lee. Although minor, the pillar height has both a qualitative and quantitative effect on snowdrifts; the differences become weaker above a certain pillar height.

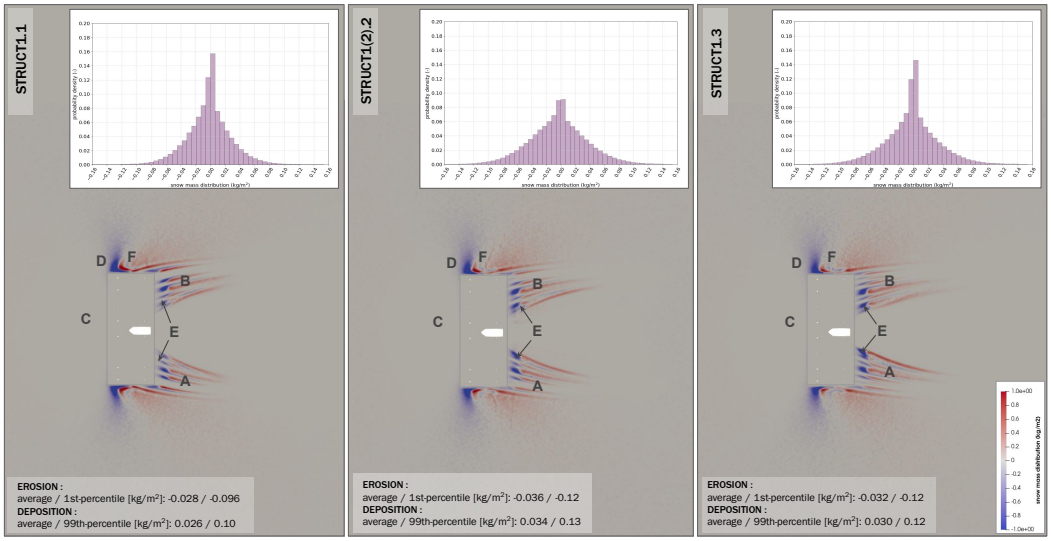

Figure 10. Snow distribution results obtained with the standard settings and: a pillar height of 4 m (STRUCT1.1), a pillar height of 6 m (STRUCT1.2) and a pillar height of 8 m (STRUCT1.3). The air flows from left to right. The top right plots show the probability distribution of snow erosion and deposition. Statistics for deposition and erosion are shown in the bottom left corner.

Staircase shape

Figure 11 shows the snow distribution results and histogram (top right) obtained in the STRUCT2 simulations. The latter aim to investigate the influence of the presence and shape of the staircase on the snow distribution. It appears that the presence of a staircase strongly influences the snowdrift structure found at Neumayer station (Figure 4.I).

Compared to the stair-free simulations (STRUCT2.1), the snow deposits into two clear zones on the lee side in all the other simulations (**A**, **B**). The STRUCT2.1 simulations look qualitatively similar to the wind-tunnel experiments obtained by Leitl et al. (2006), showing erosion zones alternating with sheltered areas into a stripped pattern. The erosion simulated at the windward corners (**D**) also appears in their experiments (Figure 9 of the article). The rectangular staircase does not significantly change the snow distribution patterns compared to the reference triangular shape (Figure 10). However, the rounded staircase (STRUCT2.4) generates distinguishable patterns from the other ones; the deposition streaks at the sides look closer to the stair-free distribution. Looking at quantities, the rectangular staircase shows both the lowest average erosion (deposition) and percentile values. The average deposition is about 40% higher in the stair-free case, which is the highest of all STRUCT2 simulations. Looking at simulations with a staircase only, the triangular shape yields the highest average snow deposition; it is about 30% and 10% higher than the rectangular and rounded staircases, respectively.

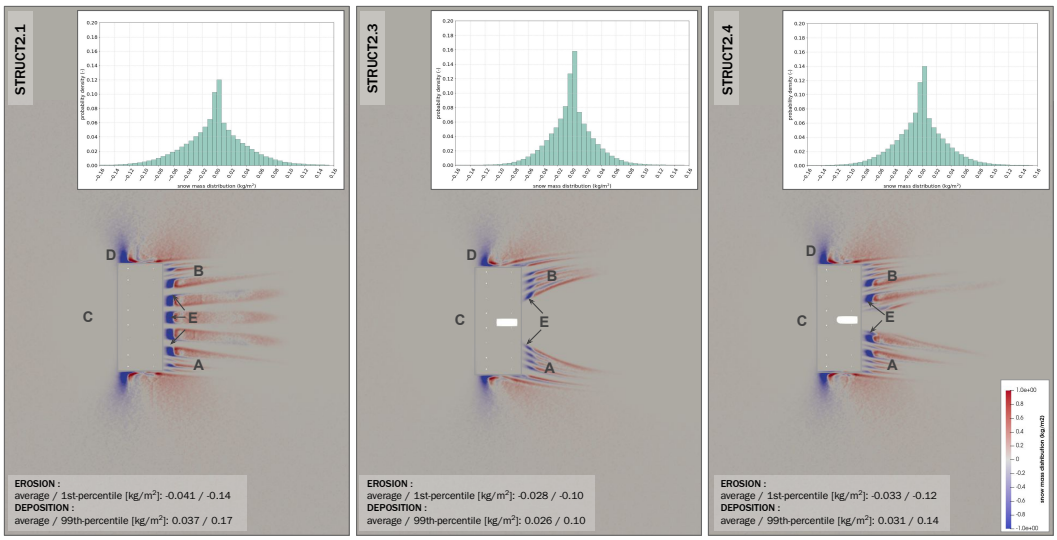

Figure 11. Snow distribution results obtained with the standard settings and: no stairs (STRUCT2.1), stairs with a rectangular shape (STRUCT2.3), stairs with a rounded shape (STRUCT2.4). The air flows from left to right. The top right plots show the probability distribution of snow erosion and deposition. Statistics for deposition and erosion are shown in the bottom left corner.

5 Discussion and Conclusion

In this work, we seek to identify the main factors influencing the formation of snowdrifts around complex structures. We ran simulations using a Eulerian-Lagrangian snow transport model (snowBedFoam) with complete surface particle dynamics for this purpose. Our simulations involve a constant numerical surface and are not yet suitable for a fully quantitative application over long time periods. However, they are able to reproduce the main components of emerging structure-borne snowdrifts and point up the influence of specific parameters on the latter. We looked at six model parameters separated in three categories, namely: (1) flow features, (2) snow properties and (3) structure design. All of them influence the location and amount of snowdrift to a certain degree; we summarize the outcome of our sensitivity study in the present section.

The effect of flow velocity was assessed by varying the friction velocity in the simulations to u* = 0.2, 0.4 and 0.6 m.s^{-1}. Wind speed largely influences the shear stress exerted by the air on the surface and the amount of particles that the flow is able to carry (Melo et al., 2022). Our simulations reveal that wind forcing has a strong influence on the location and importance of snow accumulation. Both the windward and leeward sides showed stronger, nearer and broader snow accumulation at higher friction velocities. Deposition quantities are significantly smaller for the u* = 0.2 m.s^{-1} simulations as the obtained shear stress is closer to the aerodynamic entrainment (Bagnold) threshold. Moreover, the rate of momentum decay increased with wind forcing, which concurs well with the work of Sharma et al. (2018). Hence, correctly characterizing the wind friction velocity is essential to simulate snowdrifts.

Snow-related properties showed to largely influence the amount of erosion and deposition. The interparticle cohesion energy has the most substantial impact, with a factor 40 between the mean deposition (erosion) values obtained with the minimum (ϕ = 0 J) and maximum ($\phi = 5 \times 10^{-9}$ J) bed cohesion energy. These results are in line with Comola and Lehning (2017) who showed that the number of splashed grains reduces with cohesion energy at constant impact velocity and grain diameter. Melo et al. (2022) report an increase in streamwise wind speed due to the global decrease of particles aloft in connection to greater bed cohesion energy. Our friction velocity fields support these observations and show higher friction velocity in the lee of the station for simulations with higher intercohesion energy; this in turn impacts the distribution patterns. Thus, correctly representing the snowpack properties at the surface is substantial when modeling snow transport. The spatio-temporal variation of those properties should be adequately incorporated within snowdrift simulations. The mean grain diameter mostly affects the magnitude of erosion and deposition, but not so much their location. Variations in deposition up to 25% were shown for the selected diameters. Medium-size particles (200 μm) showed the highest drift quantities, likely due to higher aerodynamic entrainment and ejection of surface grains compared to the larger and smaller grains, respectively. The last parameter we looked at in our simulations is the precipitation intensity. Injecting precipitation particles in the numerical domain mimics the effect of preferential deposition (Lehning et al., 2008) around the Neumayer structure. Expectedly, the simulations with precipitation showed a higher deposition overall in the domain, leading to a positively skewed distribution. The average deposition increases proportionally to the snowfall rate. An interesting property of preferential deposition is that it puts in evidence some flow characteristics that are overlooked in "pure" drifting snow simulations. The windward component of the snowdrift accentuates with precipitation, while it is almost non-existent with the standard settings. This improves the comparison with the measured distribution, for which the upwind deposition hill is a prominent feature. The low-velocity area upstream of the building can be reached by falling particles, which keep accumulating in this wind-sheltered area. The eastern hill at Neumayer station is expected to have grown so close to the building mainly because of precipitation. Thus, predicting snowdrifts around complex structures with accuracy must entail correct precipitation estimates.

Besides the flow and snow properties, the impact of structure design on snowdrift was numerically investigated. Our results show that the height of the pillars only slightly affects the snow distribution patterns. Variations in drift amount reach up to 30% for a 2 m height difference at the pillars. The station elevation influences the flow blockage by the building components (e.g. staircase) and the subsequent recirculation around them; this impacts the regions reached by the snow. Additionally, the presence of the staircase and its shape clearly impacted the snow distribution patterns. The staircase showed to be responsible for breaking the drift into 2 main components at the lee side. The shape of the staircase mainly influences the surface area and extent of the snow deposition at the lee; the rectangular shape yields the lowest mean deposition because it blocks the flow more heavily (lower deposition area). The more "aerodynamic" staircases such as

the rounded or triangular ones actually lead the snow to deposit on a larger area, which raises the mean deposition value. Our analysis shows that a detailed representation of building features can play a big role in the accurate prediction of snow distribution patterns around structures. Therefore, care should be taken not to overlook those key components when modeling buildings. Our results support the hypothesis of Tominaga et al. (2011) stating that small aerodynamic changes can cause significant variations in snow distribution patterns.

In general, simulating snowdrifts with numerical models is very useful to understand which processes govern their emergence. With our snow model entailing detailed surface processes, the impact of fine parameters such as grain size or bed intercohesion could be thoroughly investigated. However, identifying the key factors forming a given snow distribution in natural landscapes stays challenging. All the governing factors relating to wind, snow or structures are tightly interconnected and the snowdrifts usually originate from their cumulative effects. Moreover, it should be kept in mind that the temporal evolution of snow accumulation structures is not included in our model; having a non-varying surface is sufficient in the context of the sensitivity analysis performed in this work, but quantitatively predicting snowdrifts would require a model with a dynamic surface adaptation (Xiaoxiao & Yu, 2022). Our simulations showed that parameters such as bed intercohesion had a massive impact on the amount of transported snow; representing the snow surface properties in space and time seems of major importance to accurately predict drifted quantities. Yet, the precise link between snowbed properties and values for parameters such as bed intercohesion or shear stress threshold is not clear. An interesting approach by Sharma et al. (2019) in their cell automata model involves the use of a time-varying erodibility factor to account for the changes in snow properties. Overall, some numerical experiments are required and would generally help in the modeling of snow transport.

Eulerian-Lagrangian models for snow transport are useful to represent snow surface processes in detail, with governing equations for air and snow and precise momentum exchange representation between the two phases. Such characteristics are beneficial for snow transport prediction in urban environments (Chen & Yu, 2023). We showed in our simulations that the number of particles aloft influences the flow surface shear stress and consequent erosion in the lee of the building; capturing those effects is only possible with the inclusion of particle feedback on the airflow. However, Eulerian-Lagrangian models are computationally expensive and simpler alternatives stay valid depending on the application. Finally, as stated by Zhou and Zhang (2023), more field measurements should be conducted to validate the models. The measurements that we currently have are only valid for a semi-quantitative comparison.

Besides, the FLOW1 simulations show that large-scale turbulence is important to reproduce snowdrifts as they are found in nature (no clear streaks). Various authors proved that RANS can be successfully used in simulations of snow drifting around obstacles despite its limitations to predict turbulence and wake flow (Thiis et al., 2009; Zhou et al., 2020; Zhou & Zhang, 2023). Combining time-consuming LES with Lagrangian particle tracking to simulate snowdrift around large-scale structures would be computationally very intensive. Therefore, we chose the widely used and high-efficiency RANS method to perform snowdrift simulations around the complex Neumayer structure.

Overall, this work has put the emphasis on the key processes involved in snowdrift formation. The airflow, snow properties and structure design interact in complex ways and we showed that surface friction velocity, bed intercohesion or structure shape had an important impact on the snowdrift. Further model development should entail a precise definition of those parameters, while including a temporal evolution of the surface and its associated properties.

Appendix A Supplementary Figures

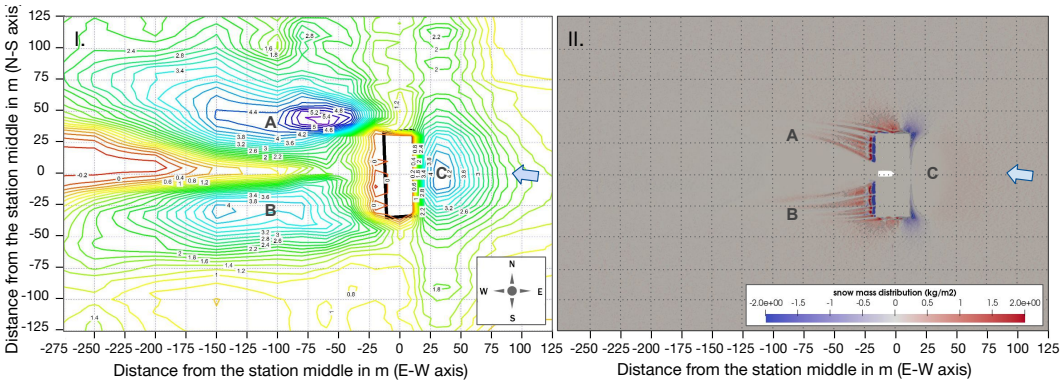

Figure A1. **I.** Characteristic snowdrift topography around Neumayer Station III, barometrically measured on June 11, 2009 over an area of 400 by 250 meters. The isolines show the topography structure in meters. **II.** Simulation results obtained with a wind speed of 10 m.s^{-1} at the inflow, the average wind direction of the most significant wind events during February to June 2009 and considering a station orientation of 356° relative to North. The wind direction is represented by the blue arrow. The snow deposition is represented in red, while the erosion is shown in blue.

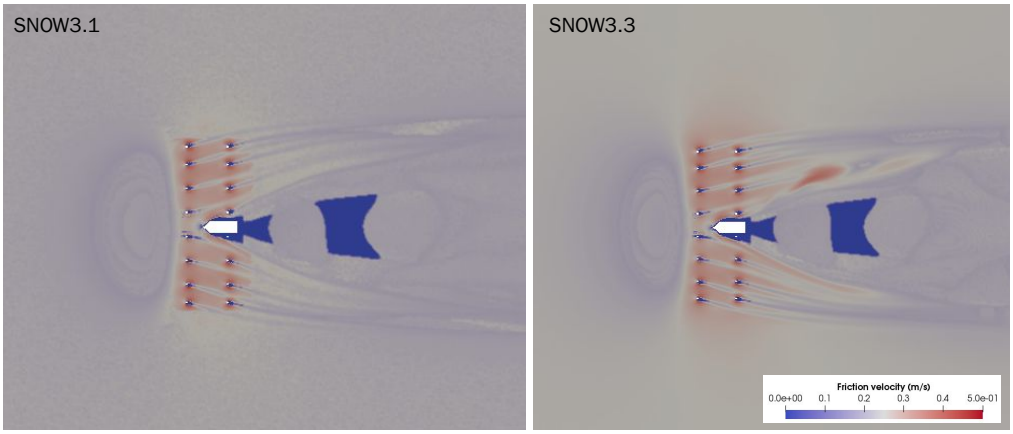

Figure A2. Surface friction velocity results obtained with the standard settings and bed inter-cohesion values of $\phi = 0$ J (SNOW3.1) and $\phi = 5 \times 10^{-9}$ J (SNOW3.3).

Open Research Section

The topographical measurements around Neumayer station and simulation results can be found on the environmental data portal EnviDat (Hames et al., 2021). The snowBedFoam code is also uploaded there (snowBedFoam-v1-5.0), in addition to being available on GitLab. Detailed information can be found directly on the portal.

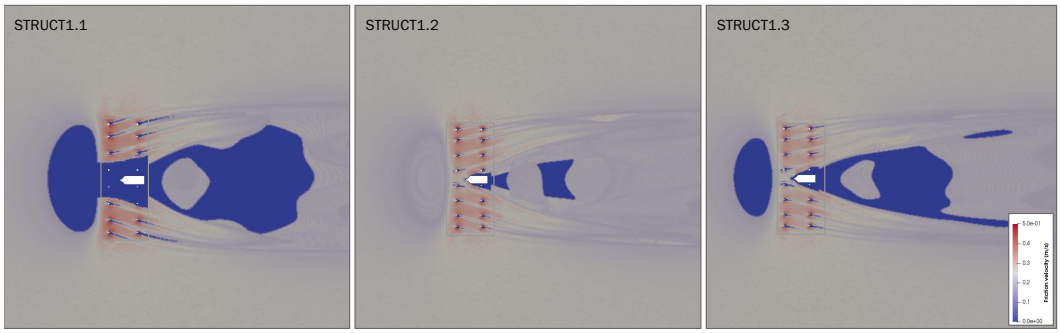

Figure A3. Surface friction velocity results obtained with the standard settings and: a pillar height of 4 m (STRUCT1.1), a pillar height of 6 m (STRUCT1.2), a pillar height of 8 m (STRUCT1.3).

Acknowledgments

The authors acknowledge the Alfred Wegener Institute, Helmholtz Centre for Polar and Marine Research for the financial and logistical support (grant number: AWI_ANT_27) as well as all the station overwinterers who took snowdrift measurements under very cold conditions. The Swiss National Supercomputing Centre (CSCS) is also acknowledged for providing the computational resources (projects s1115, s1242). The authors thank Daniela Brito Melo for her thorough insight on snow saltation mechanisms. Open access funding provided by Ecole Polytechnique Fédérale de Lausanne and the WSL Institute for Snow and Avalanche Research SLF.

References

Amory, C., Gallée, H., Naaim-Bouvet, F., Favier, V., Vignon, E., Picard, G., ... Bellot, H. (2017, July). Seasonal Variations in Drag Coefficient over a Sastrugi-Covered Snowfield in Coastal East Antarctica. *Boundary-Layer Meteorology*, *164*(1), 107–133. doi: 10.1007/s10546-017-0242-5

Anderson, R. S., & Haff, P. K. (1991). Wind modification and bed response during saltation of sand in air. In O. E. Barndorff-Nielsen & B. B. Willetts (Eds.), *Aeolian Grain Transport 1* (pp. 21–51). Vienna: Springer. doi: 10.1007/978-3-7091-6706-9_2

Bagheri Dastgerdi, S., Behrens, M., Bonne, J.-L., Hörhold, M., Lohmann, G., Schlosser, E., & Werner, M. (2021). Continuous monitoring of surface water vapour isotopic compositions at Neumayer Station III, East Antarctica. *The Cryosphere*, *15*(10), 4745–4767. doi: 10.5194/tc-15-4745-2021

Bagnold, R. A. (1941). The Physics of Blown Sand and Desert Dunes..

Bartzis, J., Vlachogianis, D., & Stefanos, A. (2004). Best Practice Advice for Environmental Flows. *TA5 QNET CFD network Newsletter*, *2*(4).

Beyers, J. H. M. (2004). Numerical modelling of the snow flow characteristics surrounding Sanae IV Research Station, Antarctica.. Retrieved from `http://hdl.handle.net/10019.1/15935`

Chen, X., & Yu, Z. (2023). Development of Eulerian–Lagrangian simulation for snow transport in the presence of obstacles. *Cold Regions Science and Technology*, *206*, 103730. doi: https://doi.org/10.1016/j.coldregions.2022.103730

Christopher J. Greenshields, CFD Direct Ltd. (2023). OpenFOAM, The OpenFOAM Foundation: User Guide (version 11). *OpenFOAM Foundation Ltd.*.

Comola, F., Giometto, M. G., Salesky, S. T., Parlange, M. B., & Lehning, M. (2019). Preferential Deposition of Snow and Dust Over Hills: Governing Processes and Relevant Scales. *Journal of Geophysical Research: Atmospheres*, *124*(14), 7951-7974. doi: https://doi.org/10.1029/2018JD029614

Comola, F., & Lehning, M. (2017). Energy- and momentum-conserving model of splash entrainment in sand and snow saltation. *Geophysical Research Letters*, *44*(3), 1601–1609. doi: 10.1002/2016GL071822

Dai, X., & Huang, N. (2014, 10). Numerical simulation of drifting snow sublimation in the saltation layer. *Scientific reports*, *4*, 6611. doi: 10.1038/srep06611

de Villiers, E. (2006). The Potential of Large Eddy Simulation for the Modelling of Wall Bounded Flows. *Cycle*.

Doorschot, J. J. J., & Lehning, M. (2002, July). Equilibrium Saltation: Mass Fluxes, Aerodynamic Entrainment, and Dependence on Grain Properties. *Boundary-Layer Meteorology*, *104*(1), 111–130. doi: 10.1023/A:1015516420286

Fernandes, C. B. P., Semyonov, D., Ferrás, L. J. L., & Nóbrega, J. M. (2018). Validation of the CFD-DPM solver DPMFoam in OpenFOAM (R) through analytical, numerical and experimental comparisons. doi: 10.1007/s10035-018-0834-x

Franke, J., & Baklanov, A. (2007). *Best Practice Guideline for the CFD Simulation of Flows in the Urban Environment: COST Action 732 Quality Assurance and Improvement of Microscale Meteorological Models*.

Franke, S., Eckstaller, A., Heitland, T., Schaefer, T., & Asseng, J. (2022, December). The role of Antarctic overwintering teams and their significance for German polar research. *Polarforschung*, *90*(2), 65–79. doi: 10.5194/polf-90-65-2022

Gromke, C., Horender, S., Walter, B., & Lehning, M. (2014). Snow particle characteristics in the saltation layer. *Journal of Glaciology*, *60*(221), 431–439. doi: 10.3189/2014JoG13J079

Groot Zwaaftink, C. D., Mott, R., & Lehning, M. (2013). Seasonal simulation of drifting snow sublimation in Alpine terrain. *Water Resources Research*, *49*(3), 1581–1590. doi: 10.1002/wrcr.20137

Hames, O., Jafari, M., & Lehning, M. (2021). *snowBedFoam: an OpenFOAM Eulerian-Lagrangian solver for modelling snow transport.* EnviDat. Retrieved from `https://www.doi.org/10.16904/envidat.223` doi: http://dx.doi.org/10.16904/envidat.223

Hames, O., Jafari, M., Wagner, D. N., Raphael, I., Clemens-Sewall, D., Polashenski, C., ... Lehning, M. (2022). Modeling the small-scale deposition of snow onto structured Arctic sea ice during a MOSAiC storm using snowBedFoam 1.0. *Geoscientific Model Development*, *15*(16), 6429–6449. doi: 10.5194/gmd-15-6429-2022

Huang, N., Yang, Y., Shao, Y., & Zhang, J. (2024, 01). Numerical simulation of falling-snow deposition pattern over 3d-hill. *Journal of Geophysical Research: Atmospheres*, *129*. doi: 10.1029/2023JD039898

Jafari, M., Sharma, V., & Lehning, M. (2022, March). Convection of water vapour in snowpacks. *Journal of Fluid Mechanics*, *934*. (Publisher: Cambridge University Press) doi: 10.1017/jfm.2021.1146

Komatsu, A., & Nishimura, K. (2022, 03). Calculation of Snowdrift Distribution over Complex Topography to Improve the Accuracy of Snow Avalanche Warning Systems. *SOLA*, *18*. doi: 10.2151/sola.2022-012

König-Langlo, G., & Loose, B. (2007). The Meteorological Observatory at Neumayer Stations (GvN and NM-II) Antarctica. *Polarforschung2006*, *76*(1), 25–38.

Kottmeier, C., & Fay, B. (1998). Trajectories in the Antarctic lower troposphere. *Journal of Geophysical Research: Atmospheres*, *103*(D9), 10947-10959. doi: https://doi.org/10.1029/97JD00768

König-Langlo, G., King, J. C., & Pettré, P. (1998). Climatology of the three coastal Antarctic stations Dumont d'Urville, Neumayer, and Halley. *Journal of Geo-*

physical Research: Atmospheres, *103*(D9), 10935-10946. doi: https://doi.org/10.1029/97JD00527

Launder, B. E., & Spalding, D. B. (1974, March). The numerical computation of turbulent flows. *Computer Methods in Applied Mechanics and Engineering*, *3*(2), 269–289. doi: 10.1016/0045-7825(74)90029-2

Lehning, M., Löwe, H., Ryser, M., & Raderschall, N. (2008). Inhomogeneous precipitation distribution and snow transport in steep terrain. *Water Resources Research*, *44*(7). doi: 10.1029/2007WR006545

Leitl, B., Schatzmann, M., Baur, T., & Koenig-Langlo, G. (2006, 06). Physical Modeling of Snow Drift and Wind Pressure Distribution at the Proposed German Antarctic Station Neumayer III. , *Volume 2: Ocean Engineering and Polar and Arctic Sciences and Technology*, 751-757. doi: 10.1115/OMAE2006-92452

Lenaerts, J. T. M., & van den Broeke, M. R. (2012). Modeling drifting snow in Antarctica with a regional climate model: 2. Results. *Journal of Geophysical Research: Atmospheres*, *117*(D5). doi: https://doi.org/10.1029/2010JD015419

Leonard, E., Qiao, H., & Nabi, S. (2021, May). A Comparison of Interpolation Methods in Fast Fluid Dynamics. *International High Performance Buildings Conference*.

Liston, G., Brown, R., & Dent, J. (1993). A two-dimensional computational model of turbulent atmospheric surface flows with drifting snow. *Annals of Glaciology*, *18*, 281–286. doi: 10.3189/S0260305500011654

Macpherson, G. B., Nordin, N., & Weller, H. G. (2009). Particle tracking in unstructured, arbitrary polyhedral meshes for use in CFD and molecular dynamics. *Communications in Numerical Methods in Engineering*, *25*(3), 263–273. doi: 10.1002/cnm.1128

Melbourne, W. H., & Styles, D. F. (1969). *Wind tunnel tests on a theory to control Antarctic drift accumulation around buildings.* Australian National Antarctic Researched Expeditions.

Melo, D. B., Sharma, V., Comola, F., Sigmund, A., & Lehning, M. (2022). Modeling snow saltation: The effect of grain size and interparticle cohesion. *Journal of Geophysical Research: Atmospheres*, *127*(1), e2021JD035260. doi: https://doi.org/10.1029/2021JD035260

Melo, D. B., Sigmund, A., & Lehning, M. (2024). Understanding snow saltation parameterizations: lessons from theory, experiments and numerical simulations. *The Cryosphere*, *18*(3), 1287–1313. doi: 10.5194/tc-18-1287-2024

Mott, R., Vionnet, V., & Grünewald, T. (2018). The Seasonal Snow Cover Dynamics: Review on Wind-Driven Coupling Processes. *Frontiers in Earth Science*, *6*.

Moukalled, F., Mangani, L., & Darwish, M. (2015). *The Finite Volume Method in Computational Fluid Dynamics: An Advanced Introduction with OpenFOAM® and Matlab®* (Vol. 113). doi: 10.1007/978-3-319-16874-6

Nishimura, K., Yokoyama, C., Ito, Y., Nemoto, M., Naaim-Bouvet, F., Bellot, H., & Fujita, K. (2014). Snow particle speeds in drifting snow. *Journal of Geophysical Research: Atmospheres*, *119*(16), 9901-9913. doi: https://doi.org/10.1002/2014JD021686

Okaze, T., Mochida, A., Tominaga, Y., Nemoto, M., Sato, T., Sasaki, Y., & Ichinohe, K. (2012). Wind tunnel investigation of drifting snow development in a boundary layer. *Journal of Wind Engineering and Industrial Aerodynamics*, *104-106*, 532-539. doi: https://doi.org/10.1016/j.jweia.2012.04.002

OpenFOAM Foundation Ltd. (2018). *OpenFOAM-5.x: source code for the Eulerian-Lagrangian solver DPMFoam.* Retrieved 2024-01-20, from `https://github.com/OpenFOAM/OpenFOAM-5.x/tree/master/applications/solvers/lagrangian/DPMFoam`

Palm, S. P., Kayetha, V., Yang, Y., & Pauly, R. (2017). Blowing snow sublimation and transport over antarctica from 11 years of calipso observations. *The Cryosphere*, *11*(6), 2555–2569. doi: 10.5194/tc-11-2555-2017

Pomeroy, J. W., & Gray, D. M. (1990). Saltation of snow. *Water Resources Research*, *26*(7), 1583-1594. doi: https://doi.org/10.1029/WR026i007p01583

Pope, S. B. (2000). *Turbulent Flows*. Cambridge University Press. doi: 10.1017/CBO9781316179475

Rasmussen, R. M., Vivekanandan, J., Cole, J., Myers, B., & Masters, C. (1999). The estimation of snowfall rate using visibility. *Journal of Applied Meteorology*, *38*(10), 1542 - 1563. doi: 10.1175/1520-0450(1999)038⟨1542:TEOSRU⟩2.0.CO;2

Schmithüsen, H. (2020). *Meteorological synoptical observations from Neumayer Station (1981-01 et seq)* [data set]. PANGAEA. doi: 10.1594/PANGAEA.911242

Schneiderbauer, S., & Prokop, A. (2011, 06). The atmospheric snow-transport model: Snowdrift3d. *Journal of Glaciology*, *57*, 526-542. doi: 10.3189/002214311796905677

Sharma, V., Braud, L., & Lehning, M. (2019). Understanding snow bedform formation by adding sintering to a cellular automata model. *The Cryosphere*, *13*(12), 3239–3260. doi: 10.5194/tc-13-3239-2019

Sharma, V., Comola, F., & Lehning, M. (2018, November). On the suitability of the Thorpe–Mason model for calculating sublimation of saltating snow. *The Cryosphere*, *12*(11), 3499–3509. (Publisher: Copernicus GmbH)

Sommer, C. G., Wever, N., Fierz, C., & Lehning, M. (2018). Investigation of a wind-packing event in Queen Maud Land, Antarctica. *The Cryosphere*, *12*(9), 2923–2939. doi: 10.5194/tc-12-2923-2018

Thiis, T., Ramberg, J., & Potac, J. (2009). 3D Numerical Simulations and Full Scale Measurements of Snow Depositions on Curved Roofs. *3D Numerical Simulations and Full Scale Measurements of Snow Depositions on Curved Roofs*, 1000–1004.

Tominaga, Y. (2018). Computational fluid dynamics simulation of snowdrift around buildings: Past achievements and future perspectives. *Cold Regions Science and Technology*, *150*, 2-14. doi: https://doi.org/10.1016/j.coldregions.2017.05.004

Tominaga, Y., Okaze, T., & Mochida, A. (2011). CFD modeling of snowdrift around a building: An overview of models and evaluation of a new approach. *Building and Environment*, *46*(4), 899-910. doi: https://doi.org/10.1016/j.buildenv.2010.10.020

Uematsu, T., Nakata, T., Takeuchi, K., Arisawa, Y., & Kaneda, Y. (1991). Three-dimensional numerical simulation of snowdrift. *Cold Regions Science and Technology*, *20*(1), 65-73. doi: https://doi.org/10.1016/0165-232X(91)90057-N

Wesche, C., Weller, R., König-Langlo, G., Fromm, T., Eckstaller, A., Nixdorf, U., & Kohlberg, E. (2016, August). Neumayer III and Kohnen Station in Antarctica operated by the Alfred Wegener Institute. *Journal of large-scale research facilities JLSRF*, *2*, A85–A85. doi: 10.17815/jlsrf-2-152

Xiaoxiao, C., & Yu, Z. (2022, 02). Driftscalardyfoam: An openfoam-based multi-stage solver for drifting snow and its distribution around buildings. *Frontiers in Earth Science*, *10*. doi: 10.3389/feart.2022.822140

Zhou, X., & Zhang, T. (2023). A review of computational fluid dynamics simulations of wind-induced snow drifting around obstacles. *Journal of Wind Engineering and Industrial Aerodynamics*, *234*, 105350. doi: https://doi.org/10.1016/j.jweia.2023.105350

Zhou, X., Zhang, Y., Kang, L., & Gu, M. (2020). RANS CFD simulations can be successfully used for simulating snowdrift on roofs in a long period of snowstorm. In *Building simulation* (Vol. 13, pp. 1157–1163).